proaches M_{w2}.[3] Thus, their exponent, 2.3, might increase if we evaluate it only from the data for the blends with $M_{w2} \gg M_{w1}$: If $M_{w2} = 270 \times 10^4$, the second term in eq 6 overwhelms the first term almost completely and the power-law type relation $\langle r_2^2 \rangle / D_{2,bB} \propto M_{w1}^3$ prevails in the range $M_{w1} \lesssim 10^5$. If we use the $\bar{\tau}$ data (Table II in ref 19) in this range of M_{w1}, the exponent becomes 2.7.

(18) Klein, J. *Macromolecules* **1986**, *19*, 105.
(19) Montfort, J.-P.; Marin, G.; Monge, P. *Macromolecules* **1984**, *17*, 1551.
(20) See, for example: Graessley, W. W. *Adv. Polym. Sci.* **1974**, *16*.
(21) Allen, V. R.; Fox, T. G. *J. Chem. Phys.* **1964**, *41*, 337.
(22) Doi, M.; Edwards, S. F. *J. Chem. Soc., Faraday Trans. 2* **1978**, *74*, 1789, 1802, 1818.
(23) However, there still remains a crucial problem: Viscoelastic properties of well-entangled polymers cannot be described by the reptation mechanism alone. If we wish to explain the viscoelastic and diffusion properties of well-entangled polymers by the generalized tube model, we must assume some other mechanisms contributing largely to viscoelastic relaxation but only slightly to diffusion. Modified theories incorporating reptation and other mechanisms (such as contour length fluctuation) were proposed to explain the viscoelastic properties.[7,24] However, most of those theories assumed the independence of competing mechanisms and were not based on the Langevin equation describing the motion of the chain segments due to those mechanisms operating simultaneously. Thus, it cannot be concluded yet that the modified theories explain the diffusion and viscoelastic properties in a unified manner.
(24) Lin, Y.-H. *Macromolecules* **1984**, *17*, 2846.
(25) Although eq 4 was determined from the D_m data for $M_w > (2–3)M_c°$, the data for $M_c° < M_w < (2–3)M_c°$ are not largely different from those calculated by eq 4, as can be seen from Figure 2. Thus, we used eq 4 to evaluate $D_{1,bB}$ for $M_{w1} > M_c°$.
(26) Miyaki, Y. Ph.D. Dissertation, Osaka University, Osaka, Japan, 1981.
(27) Watanabe, H.; Kotaka, T. *Macromolecules* **1986**, *19*, 2520.
(28) $\langle r_2^2 \rangle^{1/2}$ of the PS chain with $M_{w2} = 52 \times 10^4$ in a Θ-solvent (cyclohexane) is smaller by a factor of 30% than that in a good solvent (benzene).[26] Thus, the difference in the $\langle r_2^2 \rangle^{1/2}$ values for the blends examined in Figure 5 would be smaller than 30% and can be neglected.
(29) Yamakawa, H. *Modern Theory of Polymer Solutions*; Harper & Row: New York, 1971.
(30) Graessley, W. W., personal communication, 1986.
(31) Smith and co-workers[32] examined the diffusion of the infinitely dilute 2-chain in the blends of poly(propylene oxide) (PPO): We found that the product $D_{2,bB}\eta_{1,m}$ (evaluated from the $\eta_{1,m}$ and $D_{2,bB}$ data in Table I and Figure 6 in their paper) was nearly the same for $M_{w1} = 1000$ and 1960. However, we also noted that $D_{2,bB}\eta_{1,m}$ for $M_{w1} = 4200$ ($< M_c° = 7000$ for PPO)[32] was significantly larger than those for $M_{w1} = 1000$ and 1960. Thus, for the PPO/PPO blends, Zimm behavior may have been observed for very small M_{w1} but not in the entire range of $M_{w1} < M_c°$. This result is consistent with those for the PS/PS blends shown in this paper (Table II).
(32) Smith, B. A.; Samulski, E. T.; Yu, L.-P.; Winnik, M. A. *Macromolecules* **1985**, *18*, 1901.

Entanglements in Binary and Ternary Blends of Narrow Molecular Weight Distribution Polystyrenes

Hiroshi Watanabe and Tadao Kotaka*

Department of Macromolecular Science, Faculty of Science, Osaka University, Toyonaka, Osaka 560, Japan. *Received June 17, 1986*

ABSTRACT: Viscoelastic properties of binary blends (bB) of monodisperse linear polystyrenes with low and intermediate molecular weights M_1 and M_2 (designated 1- and 2-chain, respectively) were examined and compared with those of ternary blends (tB) composed of the same 1- and 2-chains plus a third high molecular weight M_3 component (3-chain). In tB, the 3-chain content w_3 was so small that no 3–3 entanglements existed. If the content of the 2-chain w_2 was sufficiently large, the compliance J_2 and viscosity η_2 of the 2-chain in bB were proportional to w_2^{-2} and $w_2^{3.5}$, as in the case of concentrated solutions of the 2-chain in a low molecular weight solvent. The range of w_2 where these relations were observed was wider for bB with larger M_2/M_1 ratio. The relaxation time τ_3 of the 3-chain in tB was proportional to w_2^3 if M_2/M_1 and w_2 were large; this relation was not observed for small M_2/M_1 and w_2. To describe the slow relaxation behavior of the 2- and 3-chains in a unified way, we evaluated an effective entanglement spacing $\tilde{M}_{e2}$ characterizing the terminal relaxation modes of the 2-chain. $\tilde{M}_{e2}$ increased with decreasing w_2 and increasing M_2/M_1 ratio. A universal relation $\tau_3 \propto \tilde{M}_{e2}^{-3}$ with $\tilde{M}_{e2}$ being determined for the corresponding bB was found for tB with large and small M_2/M_1 ratio. Thus, bB and tB respectively could be regarded in the long-time region as the concentrated solution of the 2-chain and 3/2 blend having the effective entanglement spacing $\tilde{M}_{e2}$. These results were interpreted on the basis of the tube renewal concept.

Introduction

The effect of entanglement on the viscoelastic properties of flexible linear polymers is one of the central problems in polymer rheology. Extensive data have been accumulated for entangled polymers with both narrow and broad molecular weight distribution (MWD).[1,2] However, the detailed relaxation mechanisms of entangled polymers are not yet fully understood.

Blends composed of narrow MWD polymers are simple but important model systems for understanding this problem because such blends often exhibit relaxation modes not observable in narrow MWD polymers. Recently, we carried out a series of systematic studies[3–6] on binary blends (bB) of narrow MWD linear polystyrenes (PS) with low and high weight-average molecular weights (M_{w1} and M_{w2}, respectively). The results obtained were as follows.[3–6]

The relaxation modes of the short-chain component (hereafter designated the 1-chain) were affected by blending only slightly, while those of the long-chain component (2-chain) were strongly dependent on M_{w1} and M_{w2} as well as on the composition w_i (i = 1, 2) of the blend.

When M_{w1} was larger than the entanglement spacing M_e, a power-law type dependence of the relaxation time of the 2-chain on M_{wi} and w_i was observed for the blends under the following *extreme* conditions.

(a) If $M_{w2} >> M_{w1} > M_e$ and $w_2 < (w_2)_c$ with $(w_2)_c$ being the critical 2-chain content for onset of entanglements between the 2-chains (2–2 entanglements), the retarded Rouse-like relaxation of the 2-chain was observed at low frequencies, and its characteristic time was[5,6]

$$\tau_{12} \propto \zeta_0 w_2^0 M_{w1}^3 M_{w2}^2 M_e^{-3} \quad (1)$$

Here ζ_0 is the monomeric friction coefficient.

0024-9297/87/2220-0535$01.50/0

(b) If $M_{w2} >> M_{w1} > M_e$ and $w_2 >> (w_2)_c$, a rubbery plateau due to 2–2 entanglements was observed at still lower frequencies, and its characteristic time τ_{22} was[3,4]

$$\tau_{22} \propto \zeta_0 w_2^{1.5} M_{w1}^{0} M_{w2}^{3.5} \quad (2)$$

(c) If M_{w1} ($>M_e$) approaches M_{w2}, eq 1 and 2 were no longer valid, and τ_{22} became insensitive to w_2 and M_{w1}. The asymptotic form was speculated to be[4]

$$\tau_{22} \propto \zeta_0 w_2^{0} M_{w1}^{0} M_{w2}^{3.5} \quad (M_{w1} \to M_{w2}) \quad (3)$$

On the basis of the generalized tube model involving the reptation and tube renewal mechanisms, we interpreted the above results as follows:[3-6] In this model, the constraint on the 2-chain is replaced by a tube, and the 2-chain *can* relax by either reptation[7] or tube renewal.[8,9]

In the blends with $M_{w2} >> M_{w1} > M_e$, the lifetime of the tube due to the 1-chains is much shorter than the reptation time of the 2-chain. Thus, if $w_2 < (w_2)_c$ and no 2–2 entanglement exists, the 2-chain relaxes by tube renewal alone, exhibiting a retarded Rouse-like mode. This led to eq 1. On the other hand, if $w_2 >> (w_2)_c$, both 1–2 and 2–2 entanglements exist, and the 2-chain first relaxes partly by renewal of the tube composed of the 1-chain and afterward escapes from the remaining tube composed of other 2-chains to relax completely. Thus, at the long-time end, the 1-chains do not constrain the 2-chain. This led to eq 2.

As M_{w1} approaches M_{w2}, the renewal time of the tube composed of the 1-chains increases and finally exceeds the reptation time of the 2-chain. Then constraints due to the 1-chains remain effective even at the long-time end, and the 2-chain behaves as in its monodisperse state. This led to eq 3.

As described above, the results may be interpreted clearly only for the blends at the extreme conditions. For the blends with intermediate values of M_{w2}/M_{w1} and w_2, no simple relations such as eq 1–3 were observed. The tube renewal and reptation processes in such blends appear to have the characteristic times of the same order of magnitudes and contribute cooperatively to the slow relaxation of the 2-chain.

To describe the behavior of the blends with large and small M_{w2}/M_{w1} and w_2 in a unified manner, we extended our study to ternary blends (tB) composed of the 2/1 binary blends (bB) and a very high molecular weight third component of the weight-average molecular weight M_{w3} (designated the 3-chain) and compared their behavior with that of the precursor bB. In the tB systems examined the 3-chains were dilute, so as to entangle only with much shorter 1- and 2-chains. The relaxation rate of such a 3-chain should be determined by diffusion of the surrounding 1- and 2-chains.[10] Thus, the 3-chain can be regarded as a probe for examining the molecular motion of the 1- and 2-chains in the blends. In this paper, we present the results and discuss possible relaxation mechanisms of the constituent chains, especially of the 2-chain.

Experimental Section

Anionically polymerized narrow MWD (hereafter designated as *monodisperse*) linear polystyrene (PS) samples were used. These samples were characterized by gel permeation chromatography, as described previously.[3,4] Table I summarizes the codes and characteristics of the samples used in this study.

The blends examined were bB and tB systems of the PS samples listed in Table I. The L2810 sample was used as the 3-chain, the L315 sample was used as the 2-chain, and the L89 or L42 samples were used as the 1-chain. The 2/1 and 3/1 bB systems and the monodisperse 1- and 2-chain systems were also examined as the reference.

Table I
Characteristics of Polystyrene Samples

code[a]	$10^{-3}M_w$	M_w/M_n
L42	41.5	1.06
L89[b]	88.5	1.07
L315[b]	315	1.07
L2810[b]	2810	1.09

[a] Code number represents $10^{-3}M_w$. [b] Supplied from Toyo Soda Mfg. Co. Ltd.

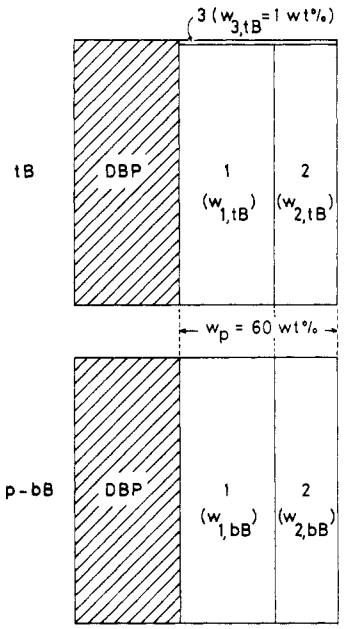

Figure 1. Schematic representation for the composition of the 3/2/1/DBP ternary and corresponding 2/1/DBP binary blends.

First, we attempted to carry out rheological measurements on tB in the molten state. However, unless the content of the 2-chain in tB was sufficiently small, the 3-chain did not relax completely at manageable temperatures ($\lesssim$220 °C) and frequencies ($\gtrsim 10^{-2}$ s^{-1}). To avoid this, we added dibutyl phthalate (DBP; Wako Pure Chemical Industries, Ltd., guaranteed grade) to the blends as a plasticizer.

Figure 1 schematically shows the composition of the 3/2/1/DBP (tB) and 2/1/DBP (bB) systems examined: DBP was always 40 wt % of the whole system, and the total polymer content w_p was 60 wt %. In tB, w_3 was always 1 wt % of the whole system, and no entanglement between the 3-chains existed.[3] These blends were prepared by the method described previously.[6] Since the densities of DBP and PS are almost the same, the weight fraction w_i of the i-chain (i = 1–3) was assumed to be equal to the volume fraction.[6]

Dynamic measurements were made at several temperatures between 10 and 120 °C with a cone-and-plate rheometer (Autoviscometer L-III, Iwamoto Seisakusho, Kyoto). The details were described previously.[3] The time–temperature superposition principle[1] was applied to the storage (G') and loss (G'') moduli.

In the following, to distinguish the quantities for the tB, bB or monodisperse (m) systems, we use a second subscript tB, bB, or m in addition to the subscript i (= 1–3) specifying the i-chain. For example, $w_{2,bB}$ represents the content of the 2-chain in bB. The second subscript will be omitted whenever possible.

Results

Figures 2 and 3 respectively show the G' and G'' curves for the L2810/L315/L42/DBP and L2810/L315/L89/DBP tB systems at 45 °C. The broken curve indicates the behavior of the 2/1/DBP system with the same w_2/w_1 ratio as that of the corresponding tB system. Such a binary blend is designated a *parent–binary blend* (p–bB) for the tB system (cf. Figure 1).

We have already carried out viscoelastic measurements on the binary blends of L2810 (3-chain in this study) and

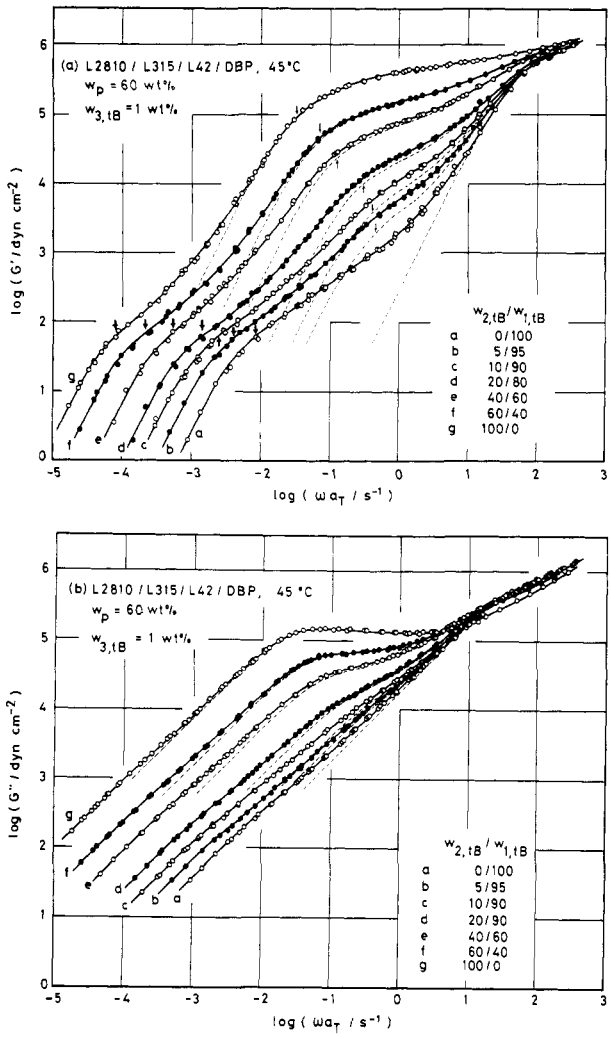

Figure 2. Master curves of (a) storage G' and (b) loss G'' moduli of L2810/L315/L42/DBP ternary blends with the total polymer content w_p = 60 wt % and the L2810 content w_3 = 1 wt % at 45 °C. The broken curves indicate the behavior of corresponding L315/L42/DBP binary blends.

low molecular weight samples with w_p = 60 wt % and w_3 = 1 wt %.[6] The relaxation time of the L2810 chain in the L2810/L42/DBP system was about 3 times longer than that in the L2810/L23/DBP system with $M_{w1} = 23.4 \times 10^3$ ($<M_e$) at an iso-ζ_0 state, for example. Thus even the shortest chain, L42, used here affected the relaxation of the L2810 chain, i.e., entangled with the L2810 chain in bB with w_p = 60 wt %.

Figure 4 shows the temperature dependence of the shift factor a_T for the bB and tB systems examined in Figures 2 and 3. These data are well described by the WLF equation[1] (solid curve)

$$\log a_T = -7.22(T - T_r)/(124.6 + T - T_r) \qquad (4)$$

with the reference temperature T_r = 45 °C. Thus, at 45 °C, all of these systems have the same free-volume-fraction f_r (=0.0601 evaluated from eq 4) and hence the same ζ_0.

As seen in Figures 2 and 3, the p–bB systems exhibit 2-step relaxation consisting of the fast and slow processes of the 1- and 2-chains. When the w_2/w_1 ratio is not very small, the G' and G'' curves of each tB at intermediate to high frequencies almost coincide with those of p–bB, indicating that the relaxation of the 1- and 2-chains in tB is nearly the same as that in p–bB. At low frequencies, the G' curve of each tB exhibits a wedgelike shoulder due to the relaxation of the 3-chain.

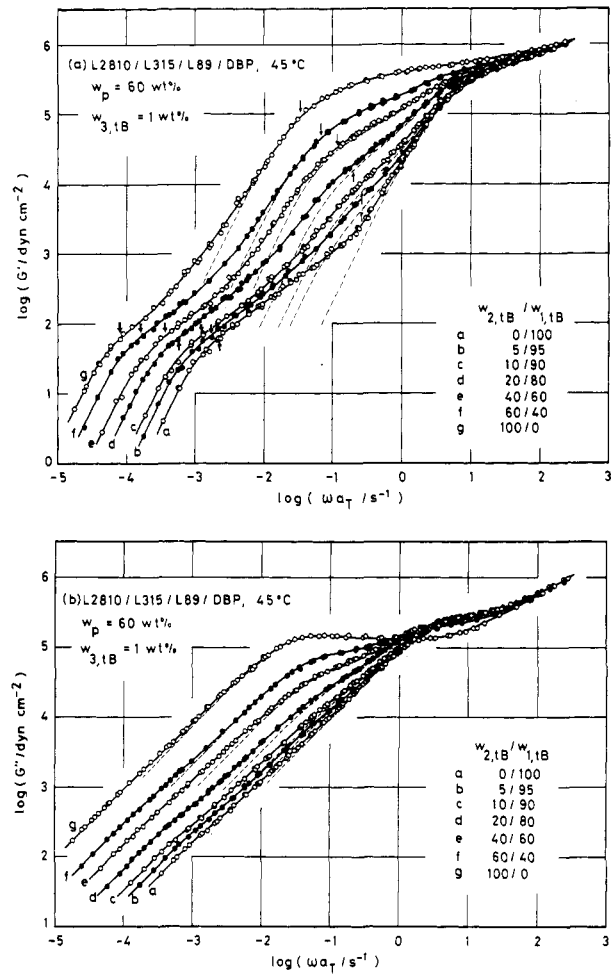

Figure 3. Master curves of (a) storage G' and (b) loss G'' moduli of L2810/L315/L89/DBP ternary blends with the total polymer content w_p = 60 wt % and the L2810 content w_3 = 1 wt % at 45 °C. The broken curves indicate the behavior of corresponding L315/L89/DBP binary blends.

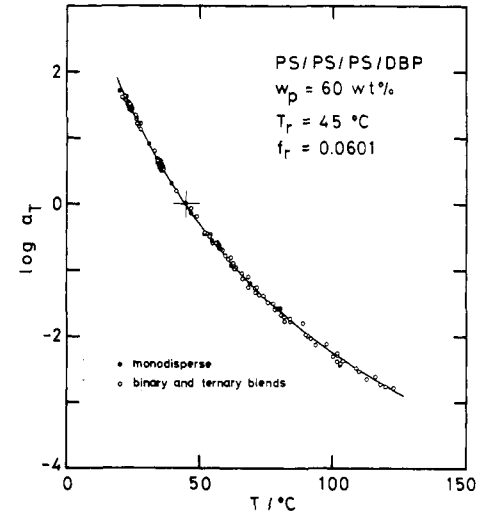

Figure 4. Temperature dependence of the shift factor a_T of the binary and ternary blends examined in Figures 2 and 3. The solid curve represents the WLF equation (eq 4) with the reference temperature T_r = 45 °C.

Analysis of the Dynamic Data. Binary Blends. To analyze the data for bB, we use the previously proposed blending law[5] for the relaxation spectra H_{bB} of bB

$$H_{bB}(\tau) = w_{1,bB}H_{1,bB}(\tau) + w_{2,bB}H_{2,bB}(\tau) \qquad (5)$$

with $H_{i,bB}$ (i = 1, 2) being the spectrum of the i-chain

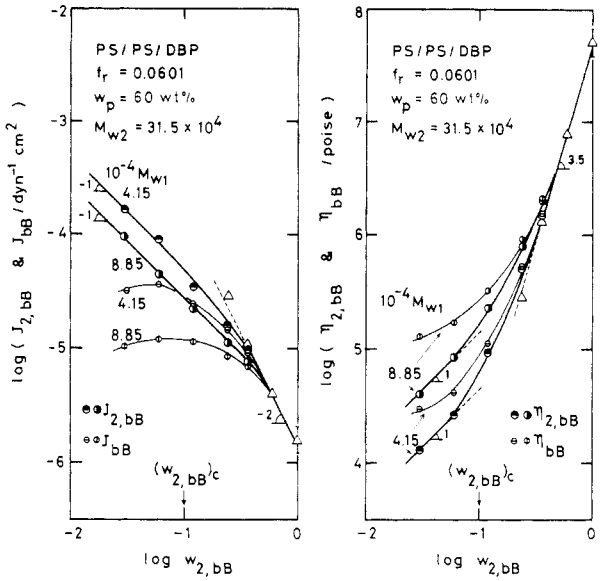

Figure 5. Dependence of the compliance $J_{2,bB}$ and viscosity $\eta_{2,bB}$ of the 2-chain (L315) in the binary blends examined in Figures 2 and 3 on the 2-chain content $w_{2,bB}$ (large half-filled circles). The small circles represent the compliance J_{bB} and viscosity η_{bB} of the binary blends. The triangles are the data for the L315/DBP solutions with the concentration $w_{2,m} = w_{2,bB}$. All these data are compared at the iso-f_r state with $f_r = 0.0601$.

(reduced to its unit volume) *in bB*. Since the behavior of the 1-chain does not differ much in bB and in its monodisperse system, we may replace $H_{1,bB}(\tau)$ by $H_{1,m}(\tau/\lambda_{1,bB})$ with $H_{1,m}(\tau)$ being the spectrum of the monodisperse 1-chain (reduced to its unit volume) in the solution with $w_{1,m}$ = 60 wt %. (This monodisperse system is designated the *parent-monodisperse* (p-m) system for the bB system.) The factor $\lambda_{1,bB}$ represents the increase in the relaxation time of the 1-chain due to blending.

Employing eq 5 and making the above replacement, we evaluated the viscosity $\eta_{2,bB}$, the elastic coefficient $A_{2,bB}$, and the compliance $J_{2,bB}$ of the 2-chain in bB directly from the data for the bB and p-m systems:

$$\eta_{2,bB} = \int_{-\infty}^{\infty} w_{2,bB}\tau H_{2,bB}\, d\ln\tau = \eta_{bB} - w_{1,bB}\lambda_{1,bB}\eta_{1,m}/w_{1,m} \quad (6a)$$

$$A_{2,bB} = \int_{-\infty}^{\infty} w_{2,bB}\tau^2 H_{2,bB}\, d\ln\tau = A_{bB} - w_{1,bB}(\lambda_{1,bB})^2 A_{1,m}/w_{1,m} \quad (6b)$$

$$J_{2,bB} = A_{2,bB}/(\eta_{2,bB})^2 \quad (6c)$$

(Here the relations $\eta_{1,m} = w_{1,m}\int_{-\infty}^{\infty}\tau H_{1,m}(\tau)\, d\ln\tau$ and $A_{1,m} = w_{1,m}\int_{-\infty}^{\infty}\tau^2 H_{1,m}(\tau)\, d\ln\tau$ were used.) The product $J_{2,bB}\eta_{2,bB}$ is the weight-average relaxation time of the 2-chain in bB. In Figures 2a and 3a, the characteristic frequencies $(J_{2,bB}\eta_{2,bB})^{-1}$ are indicated by the thin arrows.

To evaluate $\lambda_{1,bB}$, we calculated H_{bB} from the G' and G'' curves and compared the shift of the peak of H_{bB} corresponding to the relaxation of the 1-chain: $\lambda_{1,bB}$ was unity for small w_2 and increased to 2–3 at large w_2. The values of η_2, A_2, and J_2 determined by eq 6 were scarcely affected by the small ambiguity in the evaluation of $\lambda_{1,bB}$ because for bB with large w_2 (i.e., with $\lambda_{1,bB} > 1$) the second terms in eq 6a and 6b were usually much smaller than the first ones.

Figure 5 shows the w_2 dependence of $J_{2,bB}$ and $\eta_{2,bB}$ of the 2-chain at 45 °C (large half-filled circles) examined in Figures 2 and 3. The small circles indicate the compliance J_{bB} and viscosity η_{bB} of the whole bB system. The triangles are the data for 2/DBP solutions at the iso-f_r state with $f_r = 0.0601$. The arrow indicates the critical 2-chain content

$$(w_{2,bB})_c = M_c^0/M_{w2} \cong 9.8 \text{ wt \%} \quad (7)$$

above which the 2–2 entanglements exist.[3] Here M_c^0 ($\cong 31 \times 10^3$)[1] is the characteristic molecular weight for bulk PS.

In Figure 5, we see that $J_{2,bB} \propto w_2^{-1}$ and $\eta_{2,bB} \propto w_2$ for $w_2 < (w_2)_c$, similar to dilute solutions. These results indicate that no 2–2 entanglement exists and $H_{2,bB}$ does not change with w_2 in such blends. With increasing $w_2 > (w_2)_c$, $J_{2,bB}$ and $\eta_{2,bB}$ become more strongly dependent on w_2, indicating the change of $H_{2,bB}$ due to 2–2 entanglements. At sufficiently large w_2, $J_{2,bB}$ and $\eta_{2,bB}$ become proportional to w_2^{-2} and $w_2^{3.5}$, respectively, approaching the compliance and viscosity of the concentrated 2/DBP solutions (triangles). However, we also find a crossover region of w_2 where the bB system behaves as neither a dilute nor a concentrated solution. This crossover region is wider for the L315/L89/DBP system with small M_{w2}/M_{w1} ratio than for the L315/L42/DBP system, as seen more clearly for the $\eta_{2,bB}$ data. Similar results were obtained for molten PS/PS blends.[11]

Ternary Blends. To analyze the tB data, we use a blending law for H_{tB} similar to eq 5:

$$H_{tB}(\tau) = \sum_{i=1}^{3} w_{i,tB}H_{i,tB}(\tau) \quad (8)$$

Here $H_{i,tB}$ is the spectrum of the i-chain (reduced to its unit volume) in tB (i = 1–3). Since the behavior of the j-chain in the present tB system is nearly the same as that in p–bB (cf. Figures 2 and 3), we may replace $H_{j,tB}$ by $H_{j,bB}$ of the j-chain in p–bB (j = 1, 2). Thus, using the relation $w_{1,tB}/w_{1,bB} = w_{2,tB}/w_{2,bB}$ for tB and p–bB (cf. Figure 1), we obtain

$$w_{1,tB}H_{1,tB}(\tau) + w_{2,tB}H_{2,tB}(\tau) = w_{2,tB}H_{bB}(\tau)/w_{2,bB} \quad (9)$$

where the subscript bB represents the p–bB system.

Employing eq 8 and 9, we evaluated the viscosity $\eta_{3,tB}$, elastic coefficient $A_{3,tB}$, and compliance $J_{3,tB}$ of the 3-chain in tB from the quantities of tB and p–bB systems as

$$\eta_{3,tB} = \eta_{tB} - w_{2,tB}\eta_{bB}/w_{2,bB} \quad (10a)$$

$$A_{3,tB} = A_{tB} - w_{2,tB}A_{bB}/w_{2,bB} \quad (10b)$$

$$J_{3,tB} = A_{3,tB}/(\eta_{3,tB})^2 \quad (10c)$$

The product $J_{3,tB}\eta_{3,tB}$ is the weight-average relaxation time of the 3-chain in tB. The thick arrows in Figures 2a and 3a indicate the characteristic frequencies $(J_{3,tB}\eta_{3,tB})^{-1}$.

Figure 6 shows the w_2 dependence of $J_{3,tB}\eta_{3,tB}$ (small circles). The filled triangles are the data for the limiting case of tB with w_2 = 0 wt %, i.e., for 3/1/DBP systems with w_3 = 1 wt % and w_p = 60 wt %. The open triangles represent the other limiting case of tB with w_1 = 0 wt %, i.e., the 3/2/DBP systems with w_3 = 1 wt % and w_2 = 23.6–99 wt % (or w_p = 24.6–100%). All these data were compared at the iso-f_r state with $f_r = 0.0601$. Since the relaxation time of the 3-chain was too long to be determined accurately for the 3/2 (L2810/L315) system in the molten state (w_p = 100 %) as described in the Introduction, we estimated it from the previous empirical equation[5] for the molten 3/2 systems with $M_{w2} \leq 124 \times 10^3$.

We defined the critical 2-chain content *in tB* by

$$(w_{2,tB})_c = (M_c^0/M_{w2}) - w_{3,tB} \cong 8.8 \text{ wt \%} \quad (11)$$

at which the 2- and 3-chains together begin to form an entanglement network. The arrow in Figure 6 indicates $(w_{2,tB})_c$. We expect that the effect of 2–2 and 2–3 entan-

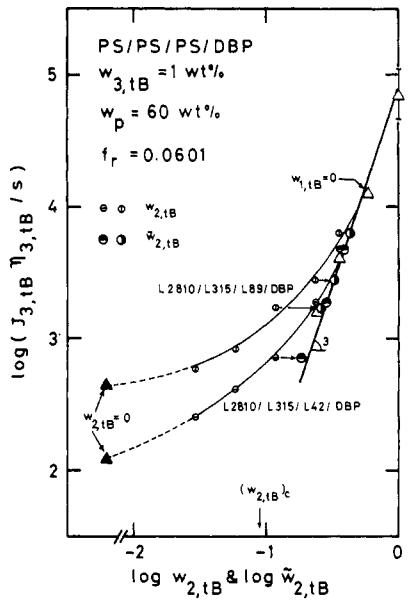

Figure 6. Dependence of the weight-average relaxation time $J_{3,tB}\eta_{3,tB}$ of the 3-chain (L2810) in the ternary blends examined in Figures 2 and 3 on the 2-chain content $w_{2,tB}$ (small circles). The filled and open triangles respectively represent the data for the 3/1/DBP and 3/2/DBP systems. The large half-filled circles are the $J_{3,tB}\eta_{3,tB}$ data plotted against the effective 2-chain content $\tilde{w}_{2,tB}$, which gives the effective entanglement spacing $\tilde{M}_{e2}$ characterizing the terminal relaxation modes of the 2-chain. All these data are compared at the iso-f_r state with f_r = 0.0601.

glements on the behavior of the 2-chain appears for $w_{2,tB} > (w_{2,tB})_c$.

As seen in Figure 6, $J_{3,tB}\eta_{3,tB}$ becomes proportional to w_2^3 and approaches the relaxation time of the 3-chain in the 3/2/DBP systems at $w_2 >> (w_2)_c$. In the range of intermediate w_2, we see a crossover region where such a simple relation is not observed. This crossover region is wider for tB with smaller M_{w2}/M_{w1} ratio. Thus, we see a clear correlation between the behaviors of tB and p–bB systems: If w_2 is sufficiently large and the 2-chain in p–bB behaves as in the 2/DBP system, the 3-chain in tB behaves as in the 3/2/DBP system.

Discussion

Effective Entanglement Spacing. As seen in Figure 6, the relaxation time of the 3-chain in tB with $w_2 > (w_2)_c$ is significantly longer than that in the 3/1/DBP system (filled triangles). This suggests that the constraints due to 1-chains disappear before the 3-chain relaxes completely and that the slow relaxation of the 3-chain in such tB is essentially affected by the 2-chains. The behavior of the 2-chain is nearly the same in tB and p–bB. Thus, using the results for p–bB shown in Figure 5 as a clue, we attempted to describe the relaxation of the 3-chain in tB with large and small M_{w2}/M_{w1} ratio in a unified way.

The results shown in Figure 5 indicate that the slow relaxation behavior of the 2-chain in bB is close to that in the concentrated 2/DBP solution only when $M_{w2} >> M_{w1}$ and $w_2 >> (w_2)_c$. This situation can be related to the change in the effective entanglement spacing $M_{e2}(t)$ for the 2-chain with time t, which is schematically shown in Figure 7.

In the short-time region (Figure 7a), the constraints due to the 1-chains are still effective and $M_{e2}(t)$ is given by

$$M_{e2}(t) = M_e^0/w_p \qquad \text{(for short } t\text{)} \tag{12}$$

where M_e^0(=18 × 10³)[1] is the entanglement spacing for bulk PS. However, such constraints become weakened and $M_{e2}(t)$ increases with t (Figure 7b) as the 1-chains diffuse

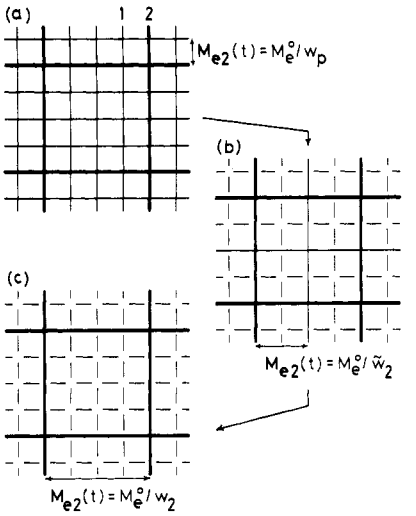

Figure 7. Schematic illustration representing the change in the effective entanglement spacing $M_{e2}(t)$ for the 2-chain in bB with time t: (a) At short t, the constraints due to the 1-chains are still effective and $M_{e2}(t) = M_e^0/w_p$; (b) $M_{e2}(t)$ increases with t; (c) $M_{e2}(t)$ asymptotically approaches the entanglement spacing M_e^0/w_2 due only to the 2–2 entanglements.

away. If we use the tube model, this process is identical with the renewal of the tube composed of 1-chains. After sufficiently long times, $M_{e2}(t)$ approaches the entanglement spacing M_e^0/w_2 for the solution of the 2-chain with the concentration w_2 (Figure 7c).

The 2-chain in bB with $M_{w2} >> M_{w1}$ and $w_2 >> (w_2)_c$ would not relax completely as $M_{e2}(t)$ has reached M_e^0/w_2. The terminal (slowest) relaxation modes of such a 2-chain are characterized by the effective mesh size M_e^0/w_2 containing no contribution of the 1-chains. That is, the 1-chains simply act as a diluent in the terminal region. On the other hand, the 2-chain in bB with intermediate M_{w2}/M_{w1} and w_2 seems to relax completely before $M_{e2}(t)$ reaches the asymptotic value M_e^0/w_2. The terminal modes of the 2-chain in this case are characterized by an effective mesh size ($<M_e^0/w_2$) to which the 1-chains are also contributing to some extent.

We know the functional form of $M_{e2}(t)$ in the entire range of t only qualitatively. However, the relaxation time of the 3-chain in tB as well as $\eta_{2,bB}$ and $A_{2,bB}$ of the 2-chain in p–bB (cf. eq 6) should be dominantly affected by the terminal modes of the 2-chain. Thus, using an effective mesh size $\tilde{M}_{e2}$ that characterizes only those terminal modes, we should be able to describe the *slow* relaxation of the 3-chain. We may assume $\tilde{M}_{e2} \cong M_{e2}(t)|_{t=J_2\eta_2}$. ($J_2\eta_2$ is close to the terminal relaxation time of the 2-chain, as shown by the thin arrows in Figures 2a and 3a.)

Here, instead of evaluating $\tilde{M}_{e2}$ itself, we define the effective 2-chain content $\tilde{w}_{2,bB}$ for p–bB by

$$\tilde{w}_{2,bB} = M_e^0/\tilde{M}_{e2} \tag{13}$$

and evaluate its value as follows: For a concentrated 2/DBP system (designated 2m system) with $w_{2,m}$ and M_e ($\propto w_{2,m}^{-1}$), the viscosity $\eta_{2,m}$ and elastic coefficient $A_{2,m}$ may be written as

$$\eta_{2,m} \propto w_{2,m}/M_e^{2.5} \propto w_{2,m}^{3.5} \tag{14a}$$

$$A_{2,m} \propto w_{2,m}/M_e^4 \propto w_{2,m}^5 \tag{14b}$$

If we regard the p–bB with $w_{2,bB} > (w_{2,bB})_c$ as a solution of the 2-chain having the mesh size $\tilde{M}_{e2}$, we obtain

$$\eta_{2,bB} \propto w_{2,bB}/\tilde{M}_{e2}^{2.5} \propto w_{2,bB}\tilde{w}_{2,bB}^{2.5} \tag{15a}$$

$$A_{2,bB} \propto w_{2,bB}/\tilde{M}_{e2}^4 \propto w_{2,bB}\tilde{w}_{2,bB}^4 \tag{15b}$$

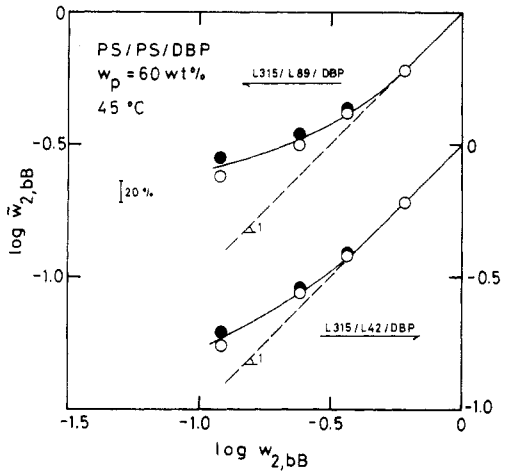

Figure 8. Comparison of the effective ($\tilde{w}_{2,bB}$) and actual ($w_{2,bB}$) 2-chain content at 45 °C in the binary blends examined in Figures 2 and 3. The open circles indicate $\tilde{w}_{2,bB}$ determined from the elastic coefficient data and the filled ones those from viscosity data.

Thus, from the data of the p–bB and 2m systems having $w_{2,m} = w_{2,bB}$ at the iso-f_r state, we can determine $\tilde{w}_{2,bB}$ as

$$\tilde{w}_{2,bB} = w_{2,bB}(\eta_{2,bB}/\eta_{2,m})^{1/2.5} \quad \text{(from eq 14a and 15a)} \tag{16a}$$

$$\tilde{w}_{2,bB} = w_{2,bB}(A_{2,bB}/A_{2,m})^{1/4} \quad \text{(from eq 14b and 15b)} \tag{16b}$$

Figure 8 compares the effective ($\tilde{w}_{2,bB}$) and actual ($w_{2,bB}$) 2-chain content for p–bB with $w_{2,bB} > (w_{2,bB})_c$. We see that $\tilde{w}_{2,bB}$ determined by eq 16a (filled circles) and eq 16b (open circles) approximately agree with each other, although a small (ca. 20%) difference is observed at small $w_{2,bB}$.[12] *As a crude approximation*, we may say that $A_{2,bB}$ and $\eta_{2,bB}$ are described by the same $\tilde{M}_{e2}$. That is, the slow relaxation modes of the 2-chain in bB may be approximated as those in an *equivalent* solution having the effective mesh size $\tilde{M}_{e2}$.

Now we turn to the tB system. The behavior of the 2-chain is nearly the same, meaning that $\tilde{M}_{e2}$ is nearly the same for the tB and p–bB systems. Thus the effective 2-chain content $\tilde{w}_{2,tB}$ for tB may be evaluated from $\tilde{w}_{2,bB}$ determined for p–bB as

$$\tilde{w}_{2,tB} = (M_e^0/\tilde{M}_{e2}) - w_{3,tB} = \tilde{w}_{2,bB} - w_{3,tB} \tag{17}$$

where $w_{3,tB}$ represents a small contribution of the 3-chain to $\tilde{M}_{e2}$ for the 2-chain in tB.

We have already shown the double-logarithmic plots of $J_{3,tB}\eta_{3,tB}$ vs. $\tilde{w}_{2,tB}$ in Figure 6 by large half-filled circles. We see that the data for tB with large and small M_{w2}/M_{w1} ratios, together with those for 3/2/DBP systems (open triangles), are reduced satisfactorily by $\tilde{w}_{2,tB}$. Thus we obtain a universal relation

$$J_{3,tB}\eta_{3,tB} \propto \tilde{w}_{2,tB}^{3} \propto \tilde{M}_{e2}^{-3} \quad (M_{w3} >> M_{w2}, M_{w1} > M_e) \tag{18}$$

for the 3-chain in the matrix of *much shorter* 1- and 2-chains. This result, together with those shown in Figure 8, indicates the validity of the concept of the effective mesh size $\tilde{M}_{e2}$ for describing the *slow* relaxation of the 2- and 3-chains in bB and tB with $w_2 > (w_2)_c$.

The 3-chain relaxes as the constraints due to much shorter 1- and 2-chains are released. Equation 18 suggests that this process may be approximated in the long-time region as the renewal of the effective entanglement network (tube) with the mesh size $\tilde{M}_{e2}$: The 3-chain relaxes as the surrounding 2-chains diffuse away in this effective network. The effect of the 1-chains appears through $\tilde{M}_{e2}$.

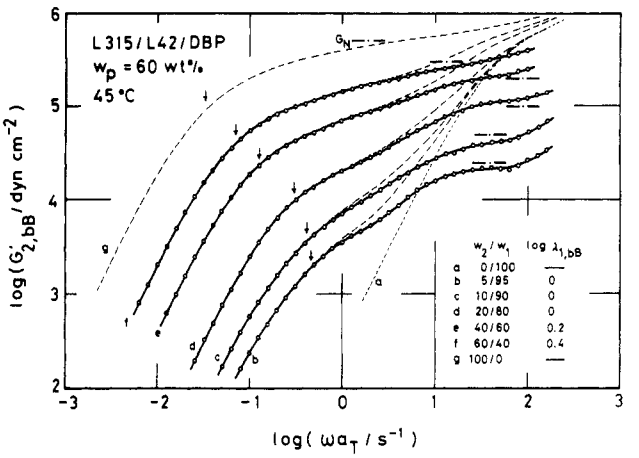

Figure 9. Master curves of the storage moduli $G_{2,bB}'$ of the 2-chain in the L315/L42/DBP systems. The broken curves represent G_{bB}'. The arrows indicate the characteristic frequencies $(J_{2,bB}\eta_{2,bB})^{-1}$, and the horizontal dash-dot lines indicate $G_N = w_2\rho RT/(M_e^0/w_p)$.

Fast Relaxation Modes of the 2-Chain in Binary Blends. Now we attempt to resolve fast modes involved in the relaxation of the 2-chain in bB. Replacing $H_{1,bB}(\tau)$ in eq 5 by $H_{1,m}(\tau/\lambda_{1,bB})$, we evaluated the complex modulus $G_{2,bB}^*$ of the 2-chain in bB from those of the bB and p–m systems as

$$G_{2,bB}^*(\omega) = G_{bB}^*(\omega) - w_{1,bB}G_{1,m}^*(\omega\lambda_{1,bB})/w_{1,m} \tag{19}$$

Figure 9 shows examples of the $G_{2,bB}'$ curves for the L315/L42/DBP systems examined in Figure 2. Two rubbery plateaus at high and low frequencies (ω) and a broad crossover region at intermediate ω are observed for bB with $w_2 > (w_2)_c$. The height of the plateau at high ω is close to $G_N = w_2\rho RT/(M_e^0/w_p)$ (horizontal dash–dot lines) with ρ being the density of bulk PS, indicating that the constraint due to 1-chains is still effective in this high ω range (cf. Figure 7a).

As shown in the previous section, the slow modes of the 2-chain in bB may be reduced to those in the *equivalent* solution with the effective mesh size $\tilde{M}_{e2}$. The plateau modulus of such a solution should be proportional to the number of effective mesh strands per unit volume, $w_2/\tilde{M}_{e2} \propto w_2\tilde{w}_2$, and the relaxation time to $\tilde{M}_{e2}^{-1.5} \propto \tilde{w}_2^{1.5}$. Thus the complex modulus $G_{2,sol}^*$ of this solution may be approximated by $G_{2,m}^*$ of the L315/DBP system with w_p = 60 wt % as[13,14]

$$G_{2,sol}^*(\omega) \cong [w_2\tilde{w}_2/w_p^2]G_{2,m}^*(\omega\tilde{w}_2^{1.5}w_p^{-1.5}) \tag{20}$$

Figure 10 compares $G_{2,sol}^*$ (broken curves) and $G_{2,bB}^*$ (solid curves) for the L315/L42/DBP bB systems with $w_2 > (w_2)_c$. The $G_{2,sol}^*$ and $G_{2,bB}^*$ curves are close to one another at low ω, but are largely different at high ω. The difference, $\Delta G_{2,bB}^* = G_{2,bB}^* - G_{2,sol}^*$, is shown by open and filled circles. These $\Delta G_{2,bB}^*$ curves exhibit a plateau and wedgelike shoulder, suggesting that the relaxation spectrum of the 2-chain in bB is boxlike at short times and wedgelike at intermediate times.

To separate the contributions of these boxlike and wedgelike components, we attempted to fit the plateau of $\Delta G_{2,bB}^*$ at high ω by an adequately shifted G^* curve of a certain monodisperse system having a boxlike spectrum.[14] We tested the values of G^* obtained experimentally so far and found that G^* of the L89/DBP system with w_p = 60 wt % gave a satisfactory fit for the bB examined in Figure 10, as shown there by the dotted curves. Hereafter, the G^* curve used for this fitting is designated $G_{2(h)}^*$: This

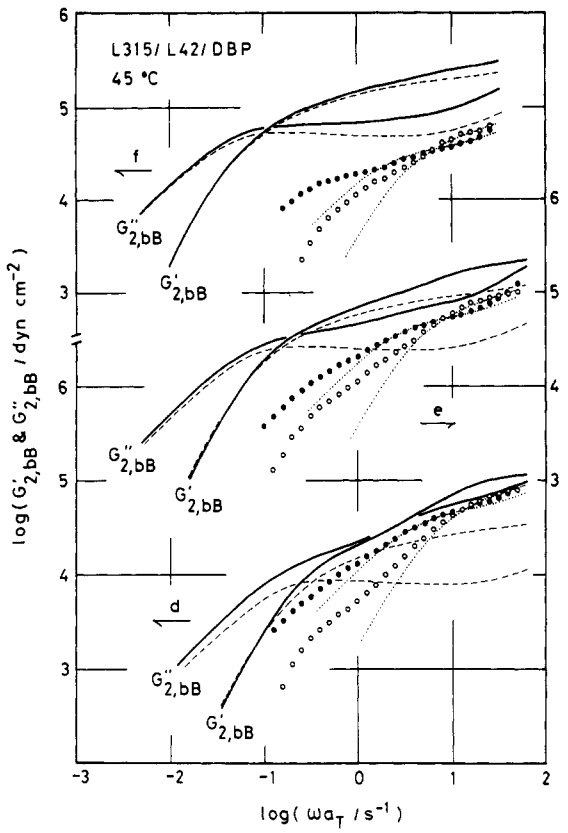

Figure 10. Comparison of the $G_{2,bB}$* (solid curves) and $G_{2,sol}$* (broken curves) for the bB systems examined in Figure 2. The w_2/w_1 ratios are 20/80, 40/60, and 60/40 for curves d, e, and f, respectively. The open and filled circles represent $\Delta G_{2,bB}'$ and $\Delta G_{2,bB}''$, respectively. The dotted $G_{2(h)}$* curves were obtained by adequately shifting the G* curve of the L89/DBP system (with w_p = 60 wt %) to fit the $\Delta G_{2,bB}$* curves at high frequencies.

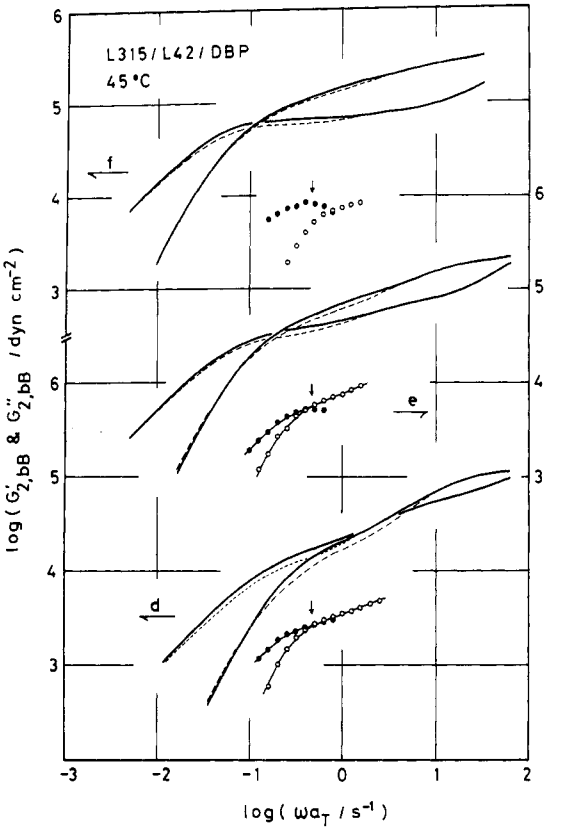

Figure 11. Comparison of $G_{2,bB}$* (solid curves) and the sum [$G_{2,sol}$* + $G_{2(h)}$*] (broken curves) for the bB systems examined in Figures 2, 9, and 10. The w_2/w_1 ratios are 20/80, 40/60, and 60/40 for curves d, e, and f, respectively. The open and filled circles represent $G_{2(i)}'$ and $G_{2(i)}''$, respectively. The arrows indicate the terminal frequency $(J_{2,bB}\eta_{2,bB})^{-1}$ of the 2-chain in bB with $w_2 < (w_2)_c$.

curve represents the contribution of the boxlike spectrum at short τ to $G_{2,bB}$*.

Figure 11 compares the sum [$G_{2,sol}$* + $G_{2(h)}$*] and $G_{2,bB}$* for the bB systems examined in Figure 10. At high and low ω, the sum (broken curves) agrees well with $G_{2,bB}$* (solid curves). However, we find a considerable difference, $G_{2(i)}$* = $G_{2,bB}$* − [$G_{2,sol}$* + $G_{2(h)}$*] (circles), between these curves at intermediate ω, suggesting a significant contribution of the intermediate modes:[15] For bB with w_2/w_1 = 20/80 (curve d), $G_{2(i)}$* is as much as 30% of the $G_{2,bB}$* and appears to be wedge-shaped. The terminal frequency of this $G_{2(i)}$* curve appears to be close to that of the 2-chain in bB with $w_2 < (w_2)_c$ indicated by the arrow.

With increasing w_2, the contribution of the intermediate modes, $G_{2(i)}$*, becomes less prominent because of the increasing contribution of the slow modes ($G_{2,sol}$*), as seen for bB with w_2/w_1 = 60/40 (curve f).

Figure 12 shows the results of a similar analysis on the L315/L89/DBP bB systems. The solid, broken, and dotted curves respectively represent $G_{2,bB}$*, $G_{2,sol}$*, and $G_{2(h)}$*, and the circles denote the sum [$G_{2,sol}$* + $G_{2(h)}$*]. The difference between the sum and $G_{2,bB}$* is small (<7%) in the entire range of ω even for the bB with w_2/w_1 = 20/80 (curve d). The wedgelike $G_{2(i)}$* curves observed for the L315/L42/DBP systems in Figure 11 were not identified here.

Relaxation Mechanisms of the 2-Chain. The results shown in Figures 10–12 may be summarized as a blending law for $H_{2,bB}$ of the 2-chain in bB

$$w_2H_{2,bB}(\tau) = H^b(\tau)|_{sh.\tau} + H^w(\tau)|_{int.\tau} + [w_2\tilde{w}_2/w_p]H_{2,m}(\tilde{w}_2^{-1.5}w_p^{1.5}\tau) \quad (5')$$

where H^b and H^w are the boxlike and wedgelike spectra at short and intermediate τ, respectively, and $H_{2,m}$ is the boxlike spectrum of the monodisperse 2-chain (reduced to its unit volume) in the L315/DBP system with w_p = 60 wt % (cf. eq 20). The first, second, and third terms correspond to $G_{2(h)}$*, $G_{2(i)}$*, and $G_{2,sol}$*, respectively. The second term is unidentifiable when M_{w1} is close to M_{w2} or w_2 is much larger than $(w_2)_c$.

We should emphasize that only the last term in eq 5′ can be evaluated from the data for monodisperse 2-chains, i.e., eq 5′ is only a *formal* blending law. However, $\eta_{2,bB}$ and $J_{2,bB}$ (and hence η_{bB} and J_{bB}) dominated by the last term may be *approximately* predicted if we know the dependence of $\tilde{w}_2$ on M_{wi} and w_i (i = 1, 2) quantitatively. In fact, Struglinski and Graessley[16] showed that the blending law for η_{bB} and J_{bB} proposed by Montfort and co-workers[17] was fairly successful, although that law contains no terms corresponding to the first and second terms in eq 5′. In other words, it is difficult to formulate the blending law for $H_{bB}(\tau)$ in the entire range of τ only from the J_{bB} and η_{bB} data, being insensitive to the fast relaxation modes.

On the basis of the generalized tube model, we may attribute the three terms appearing in eq 5′ to the different relaxation modes of the 2-chain in bB with $M_{w2} >> M_{w1} > M_e$ and $w_2 > (w_2)_c$ taking place in a stepwise manner:[3] the first and third terms to the reptation-like modes in the entanglement network with the mesh size M_e^0/w_p at short times and $\tilde{M}_{e2}$ at long times, and the second term to the Rouse-like mode due to partial tube renewal at intermediate times. Struglinski and Graessley[16] also reached a similar molecular picture (case II in Figure 17 in ref 16).

For bB with small M_{w2}/M_{w1} ratio, the second term in

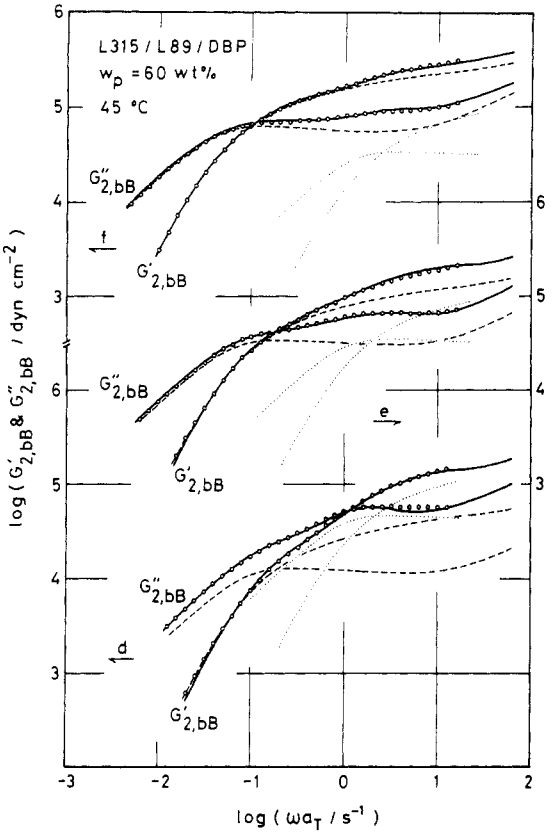

Figure 12. Comparison of $G_{2,bB}^*$ (solid curves) and $G_{2,sol}^*$ (broken curves) for the bB systems examined in Figure 3. The w_2/w_1 ratios are 20/80, 40/60, and 60/40 for curves d, e, and f, respectively. The dotted $G_{2(h)}^*$ curves were obtained by adequately shifting the G^* curve of the L315/DBP system (with w_p = 60 wt %) to fit the $\Delta G_{2,bB}^*$ curves at high frequencies. The circles represent the sum $[G_{2,sol}^* + G_{2(h)}^*]$.

eq 5′ vanishes and the intensity of the third term ($\propto w_2\tilde{w}_2$) is larger than that ($\propto w_2^2$) for the solution (cf. Figures 8 and 12). The partial tube renewal and reptation modes seem to take place cooperatively, merging into a single mode at long times.

Here we examine the partial tube renewal time in bB with $M_{w2} >> M_{w1}$ and $w_2 > (w_2)_c$. If the Rouse-like motion of the 2-chain due to partial tube renewal is confined between the adjacent 2–2 entanglement points, its characteristic time should decrease with increasing w_2 and differ largely from the tube renewal time for $w_2 < (w_2)_c$. However, as can be seen from Figure 11, the characteristic times of the $G_{2(i)}^*$ curves due presumably to partial tube renewal appear to be little dependent on w_2 and close to the relaxation time of the 2-chain (tube renewal time) in bB with $w_2 < (w_2)_c$ (cf. the arrows): The molecular motion not confined between the 2–2 entanglement points might emerge during the partial tube renewal process.[18] Further study is necessary on this problem.

Acknowledgment. We acknowledge with thanks the financial support of the Ministry of Education, Science, and Culture (Mombusho), Japan under Grant 60470107. We also thank Dr. Mitsutoshi Fukuda, Toyo Soda Mfg. Co. Ltd., for supplying us with most of the PS samples used.

List of Symbols

bB, tB: binary and ternary blends
M_e^0, M_c^0: entanglement spacing and characteristic molecular weight for bulk PS
ζ_0: monomeric friction coefficient
f_r: free-volume fraction
M_{wi}: weight-average molecular weight of i-chain (i = 1–3)
$w_{i,X}$: content of i-chain in monodisperse (X = m), bB (X = bB), and tB (X = tB) systems (i = 1–3)
w_p: total polymer content
$(w_{2,bB})_c$: critical 2-chain content for the onset of the 2–2 entanglements in bB
$(w_{2,tB})_c$: critical 2-chain content at which the 2- and 3-chains in tB together begin to form the entanglement network
H_{bB}, H_{tB}: relaxation spectra of bB and tB
$H_{i,X}$: relaxation spectrum of i-chain reduced to its unit volume in monodisperse (X = m), bB (X = bB), and tB (X = tB) systems (i = 1–3)
τ: relaxation time
$\lambda_{1,bB}$: factor representing the increase in the relaxation time of the 1-chain due to blending
$\eta_{i,X}$, $A_{i,X}$, $J_{i,X}$: viscosity, elastic coefficient, and compliance of the i-chain in monodisperse (X = m), bB (X = bB), and tB (X = tB) systems (i = 1–3)
η_X, A_X, J_X: viscosity, elastic coefficient, and compliance of bB (X = bB) and tB (X = tB) systems
$M_{e2}(t)$: time-dependent effective entanglement spacing for the 2-chain in bB and tB
$\tilde{M}_{e2}$: effective entanglement spacing that characterizes only the terminal relaxation modes of the 2-chain
$\tilde{w}_{2,bB}$, $\tilde{w}_{2,tB}$: effective 2-chain content corresponding to $\tilde{M}_{e2}$ in bB and tB
ω: frequency
G_{bB}^*: complex moduli of bB
$G_{i,m}^*$: complex moduli of monodisperse i-chain (i = 1–3)
$G_{2,bB}^*$: complex moduli of the 2-chain in bB (cf. eq 19)
$G_{2,sol}^*$: complex moduli of a solution having the effective entanglement spacing $\tilde{M}_{e2}$. This quantity represents the contribution of the slow relaxation modes of the 2-chain to $G_{2,bB}^*$. (cf. eq 20)
$\Delta G_{2,bB}^*$: contribution of the fast and intermediate modes of the 2-chain to $G_{2,bB}^*$; $\Delta G_{2,bB}^* = G_{2,bB}^* - G_{2,sol}^*$
$G_{2(h)}^*$: contribution of the fast relaxation modes of the 2-chain to $G_{2,bB}^*$
$G_{2(i)}^*$: contribution of the intermediate relaxation modes of the 2-chain to $G_{2,bB}^*$; $G_{2(i)}^* = G_{2,bB}^* - [G_{2(h)}^* + G_{2,sol}^*]$
H^b: boxlike relaxation spectrum of the 2-chain at short τ corresponding to $G_{2(h)}^*$
H^w: wedgelike relaxation spectrum of the 2-chain at intermediate τ corresponding to $G_{2(i)}^*$

Registry No. Polystyrene, 9003-53-6.

References and Notes

(1) Ferry, J. D. *Viscoelastic Properties of Polymers*, 3rd ed.; Wiley: New York, 1980.
(2) Graessley, W. W. *Adv. Polym. Sci.* **1974**, *16*.
(3) Watanabe, H.; Kotaka, T. *Macromolecules* **1984**, *17*, 2316.
(4) Watanabe, H.; Sakamoto, T.; Kotaka, T. *Macromolecules* **1985**, *18*, 1008.
(5) Watanabe, H.; Sakamoto, T.; Kotaka, T. *Macromolecules* **1985**, *18*, 1436.
(6) Watanabe, H.; Kotaka, T. *Macromolecules* **1986**, *19*, 2520.
(7) Doi, M.; Edwards, S. F. *J. Chem. Soc., Faraday Trans. 2* **1978**, *74*, 1789; **1978**, *74*, 1802; **1978**, *74*, 1818.
(8) Klein, J. *Macromolecules* **1978**, *11*, 852.
(9) Graessley, W. W. *Adv. Polym. Sci.* **1982**, *47*.
(10) Watanabe, H.; Kotaka, T. *Macromolecules*, in press
(11) Watanabe, H.; Kotaka, T. *J. Soc. Rheol. Jpn.*, in press.
(12) Although both $\eta_{2,bB}$ and $A_{2,bB}$ are determined essentially by the slow (terminal) modes, the fast modes found in Figures 9–12 also contribute to some extent to these quantities: $A_{2,bB}$ is less sensitive to such fast modes than $\eta_{2,bB}$. Thus, a small difference was observed between $\tilde{w}_2$ evaluated from $A_{2,bB}$ and $\eta_{2,bB}$ for small w_2 in Figure 8, although we neglected it in the subsequent analysis. This difference vanishes for large w_2 because

there the slow modes overwhelm the fast ones completely.
(13) $\tilde{w}_2$ determined from the A_2 data was used to evaluate $G_{2,sol}^*$ because A_2 is less sensitive to the fast relaxation modes than η_2.[12]
(14) Both slow and fast modes contribute to the *empirically determined* $G_{2,m}^*(\omega)$, although the contribution of the fast modes is not significant at low ω. Thus, some fast modes, which should contribute to $\Delta G_{2,bB}^*$, were lost from $\Delta G_{2,bB}^*$ as $G_{2,sol}^*$ represented by $G_{2,m}^*$ (eq 20) was subtracted from $G_{2,bB}^*$. (Analyzing the spectra H_{bB} itself, we can avoid this difficulty.[3,4]) However, in practical purposes, this problem is not serious in the present analysis on bB with small w_2 (curves d in Figures 10 and 12) because $G_{2,sol}^*$ is already much smaller than $G_{2,bB}^*$ at high ω: The $\Delta G_{2,bB}^*$ curve would not change much even if we use the $G_{2,sol}^*$ to which only the slow modes contribute.
(15) For bB with much larger M_{w2}/M_{w1} ratio we observed the wedge-shaped $G_{2(i)}^*$ curve more clearly.[11]
(16) Struglinski, M. J.; Graessley, W. W. *Macromolecules* **1985**, *18*, 2630.
(17) Montfort, J.-P.; Marin, G.; Monge, P. *Macromolecules* **1984**, *17*, 1551.
(18) The characteristic time of the $G_{2(i)}^*$ curve increases with increasing M_{w2}.[11] This result also suggests that the Rouse-like motion of the 2-chain due to partial tube renewal is not confined between the adjacent 2–2 entanglement points.

Flexible Polymers with Excluded Volume at a Penetrable Interacting Surface

Jack F. Douglas,* Shi-Qing Wang, and Karl F. Freed

The James Franck Institute and Departments of Chemistry and Physics, The University of Chicago, Chicago, Illinois 60637. *Received August 18, 1986*

ABSTRACT: Polymers, terminally attached to a $d_\parallel$-dimension penetrable interacting hypersurface, are described by using the two-parameter model of excluded volume, a pseudopotential polymer–surface interaction model, and the renormalization group method. The dimensionality of the hypersurface is fixed as $d_\parallel = 2$, so that the ϵ-expansion ($\epsilon = 4 - d$ with d the dimension of space) method can be applied to both the polymer–polymer and polymer–surface interactions. Then the mean-square end-to-end vector distance $\langle \mathbf{R}^2 \rangle$ is calculated to first order in ϵ as a function of polymer–surface and polymer–polymer interactions. The result is compared to $\langle \mathbf{R}^2 \rangle$ for a terminally attached polymer at an impenetrable interacting surface. An increase in the chain expansion due to *repulsive* excluded volume interactions leads to a *decrease* in the effects of repulsive polymer–surface interactions on the polymer dimensions. This phenomenon is an apparent consequence of the lower density of the chain upon expansion and the resultant lower probability of the chain encountering the surface. Scaling arguments, on the other hand, indicate that *attractive* surface interactions *amplify* the effect of the excluded volume interaction.

I. Introduction

The theoretical description of isolated polymers in the presence of an interacting boundary has been considered by using both lattice random walk and continuum random walk models. Rubin[1] has studied lattice random walks interacting with an impenetrable surface for the full range of the polymer–surface interaction and has calculated many of the important configurational properties of ideal polymers with no polymer–polymer interactions. de Gennes[2] and Lêpine and Caillé[3] have also made important contributions to the continuum formulation of the random walk model of a chain interacting with an impenetrable surface.

Some recent work has focused on extending these earlier calculations to consider penetrable surfaces. Hammersley et al.[4] give exact lattice random walk model calculations for an interacting penetrable surface. Kosmas[5] introduces a continuum model of a Gaussian polymer interacting with a penetrable surface of continuously variable dimension $d_\parallel$, and Nemirovsky and Freed[6] consider the exact analytic treatment of the special case of penetrable and impenetrable surfaces having a dimension one less than that of the embedding space, $d_\parallel = d - 1$. More recently, Douglas et al.[7] studied the exact treatment of the penetrable interacting surface model[5] for Gaussian chains where the adsorbing surface dimension $d_\parallel$ is a variable. Wang et al.[8] generalize the Nemirovsky and Freed[6] calculation by including three surface interactions, one for each side of the surface and one describing the "penetrability" of the surface. The penetrable surface model[5,7] with variable $d_\parallel$ can be similarly extended to include three surface interaction parameters, but this is left for future work.

The introduction of polymer–polymer excluded volume interactions is an important extension of the lattice random walk and continuous Gaussian chain models. Hammersley et al.[4] perform exact calculation for lattice self-avoiding walks (SAW's) for both penetrable and impenetrable surfaces, and there are numerous Monte Carlo and direct enumeration calculations[9] for SAW's interacting with an impenetrable surface. Recent lattice calculations by Ishinabe[10] and Kremer[11] consider SAW's interacting with a penetrable surface.

The development of renormalization group (RG) methods enables the extension of surface-interacting Gaussian chain models to incorporate the excluded volume interaction, provided the polymer–polymer interactions are not strongly attractive.[7,12] The first extensive treatment of surface-interacting polymers by Eisenriegler et al.[13] uses the polymer–magnet analogy in conjunction with Monte Carlo and scaling methods to consider numerous properties of surface-interacting polymers. Freed[14] employs the equivalent two-parameter (TP) model of excluded volume and evaluates some basic radial properties such as $\langle \mathbf{R}^2 \rangle$ and the end-to-end vector distribution function for a polymer at an impenetrable reflecting surface where the polymer–surface interaction vanishes. Eisenriegler[15] calculates some similar properties in this limit within the magnetic analogy model and also considers the concentration dependence of polymers near impenetrable surfaces. Nemirovsky and Freed[6] generalize the TP approach to treat the full "double crossover dependence" of polymer properties on the polymer–polymer and polymer–surface

0024-9297/87/2220-0543$01.50/0